

UC Santa Cruz

UC Santa Cruz Electronic Theses and Dissertations

Title

Quantifying Regional Variation of Structural Maps in the Neonatal Mouse Cortex

Permalink

<https://escholarship.org/uc/item/8n7308qj>

Author

Lamb, Jacqueline Elizabeth

Publication Date

2019

Copyright Information

This work is made available under the terms of a Creative Commons Attribution License, available at <https://creativecommons.org/licenses/by/4.0/>

Peer reviewed|Thesis/dissertation

UNIVERSITY OF CALIFORNIA

SANTA CRUZ

**QUANTIFYING REGIONAL VARIATION OF STRUCTURAL MAPS IN
THE NEONATAL MOUSE CORTEX**

A thesis submitted in partial satisfaction
of the requirements for the degree of

MASTER OF ARTS

in

MOLECULAR, CELL AND DEVELOPMENTAL BIOLOGY

by

Jacqueline Lamb

March 2019

The Thesis of Jacqueline Lamb is

approved:

Professor James Ackman, Chair

Professor Bin Chen

Professor David Feldheim

Lori Kletzer
Vice Provost and Dean of Graduate
Studies

TABLE OF CONTENTS

Figure	Page
LIST OF FIGURES	v
LIST OF TABLES	vi
ABSTRACT.....	vii
ACKNOWLEDGEMENTS	viii
CHAPTER	
1. BACKGROUND	1
a. Introduction	1
b. The Mouse as a Model Organism	2
c. Arealization of the Cortex	6
d. <i>In Vivo</i> Functional Recordings Using Calcium Imaging Techniques	7
e. Functional Mapping – ICA and Domain Segregation.....	11
f. Mapping Regional Cytoarchitecture of Neonatal Mice	13
g. Thesis Overview.....	16
2. METHODS.....	17
a. Snap25-GCaMP6s Transgenic Mice	17
b. Functional Data Acquisition.....	17
c. ICA and Domain Mapping of Functional Brain Data	19
d. Mapping Regional Cytoarchitecture with WISH.....	19
i. Brain preparation	19
ii. Probe design.....	20
iii. WISH.....	21
3. QUANTIFYING REGIONAL STRUCTURAL VARIATION	24
a. Introduction.....	24
b. Results.....	24
i. Structural Mapping with WISH	24
ii. Quantification of Regional Map Variation.....	25
c. Discussion	31
i. Potential Sources of Variation.....	31
ii. Analysis of Angles and Distances from Origin to Characteristic Points	33
iii. Analysis of Bounding Box Graphs.....	34

4. FUTURE DIRECTIONS.....	39
a. LNA Probes: Various Ages and Molecules of Interest	39
b. Genotypic Models of Abnormal Brain Development.....	39
c. Aligning Functional and Structural Maps.....	40
APPENDIX	
A. SUPPLEMENTAL DATA AND FIGURES	44
REFERENCES	52

LIST OF FIGURES

Figure	Page
Figure 1. Comparative brain homology of the human and rodent brains.....	5
Figure 2. GCaMP activation in calcium imaging.	9
Figure 3. Generation of wild-type and Snap25-GCaMP6s transgenic mouse lines.	10
Figure 4. Creation of functional structure maps by ICA and domain analysis.	12
Figure 5. Functional Imaging Set-Up.....	18
Figure 6. Structural maps produced by WISH.	27
Figure 7. Designing parameters for structural map measurements.	28
Figure 8. Quantifying length and angle variation from reference midpoint to characteristic edge points of ROIs.	29
Figure 9. Quantifying medial-lateral and anterior-posterior distance variation of regional bounding boxes with respect to origin axis.	30
Figure 10. Comparing functional and structural map variation.....	42

LIST OF TABLES

TABLE	Page
Table 1. Brain weights of individual animals from each litter.....	38
Table 2. Sample data from P5 functional map.....	43

**QUANTIFYING REGIONAL VARIATION OF STRUCTURAL MAPS IN
THE NEONATAL MOUSE CORTEX**

by

Jacqueline Lamb

ABSTRACT

Cortical brain regions are functionally specialized and therefore display unique cytoarchitecture. The question of how these regions develop both structurally and functionally represents the basis of important neuroscientific research. To study the development of neuronal function, calcium imaging of GCaMP6s reporter mice was performed and recorded. The recordings of functional activity patterns were analyzed for the creation of functional maps. Cytoarchitectural boundaries of regions of interest were then structurally mapped using whole-mount in situ hybridization with digoxigenin (DIG)-labeled probes to mark molecules of interest involved in early cortical organization. The regional variance of structural maps was measured to provide a framework for comparison of function data at a specified point in development to investigate the hypothesis that functional maps are predictive of underlying anatomical structure.

ACKNOWLEDGEMENTS

I would like to acknowledge and thank Dr. James Ackman for his incredible amount of support and insight throughout this entire process. It has been an honor and a privilege to be able to work in Dr. Ackman's laboratory alongside excellent lab members, who have been wonderful friends throughout the years.

I would like to thank my committee members Dr. David Feldheim and Dr. Bin Chen for their assistance and feedback during this process.

Thank you to my family who have been encouraging and uplifting throughout it all. I would not have been able to do it without your patience and support.

CHAPTER 1

BACKGROUND

a. Introduction

The nervous system's underlying organization determines its function. Neurons are highly active during the process of early development, and their wiring early on shapes the brain circuitry required for complex brain functioning in adulthood. The brain self-assembles through two simultaneous processes. First, molecular gradients and trophic factors set up the functional organization that reflects distinct arrangements of axonal connections (McLaughlin, Torborg, Feller, & O'Leary, 2003). Second, the brain undergoes circuit maturation in an activity-dependent manner as a method of regulating sensory network development. The display of spontaneous activity in early development is an emergent property of the immature nervous system that is thought to mediate synaptic competition and instruct the brain's self-organization. (Ackman et al., 2012) A great interest in neuroscience is how to create a comprehensive set of developmental maps of the mouse cortex during normal early development from both functional and structural standpoints. Understanding the activity changes that accompany synapse and circuit formation is important to understanding the mechanisms by which activity molds circuits and would help to identify critical checkpoints for normal development (Shen & Colonnese, 2016). If a normal developmental profile of the cortex is created, it can be used to be able to study the functional and structural implications in models for any number of genetic or environmental disorders in human brain development.

To understand the underlying basis of cortical development, the correlation between changes in neuronal function and regional cortical development must be investigated. In the following experiments, spontaneous activity in the developing brain was recorded *in vivo* using mesoscale calcium imaging (Ackman et. al, 2014). With this method, a genetically encoded calcium indicator was used to indirectly measure action potentials through calcium flux to study neuronal activity. Functional domain maps were subsequently generated from functional recordings by independent component analysis and domain segregation across the cortex. Mapping of cytoarchitectural boundaries of regions of interest within the cortex was performed using whole-mount in situ hybridization (WISH) with digoxigenin-labeled probes. WISH protocols produced structural maps which were analyzed and measured to provide a spatial framework for the quantification of variance of the underlying state of organization of the brain at a specified point in development. Maps of regional cytoarchitectonic boundaries serve as a point of comparison for the generated maps of functional structure at the same age to investigate the hypothesis that functional maps are predictive of underlying anatomical structure.

b. The Mouse as a Model Organism

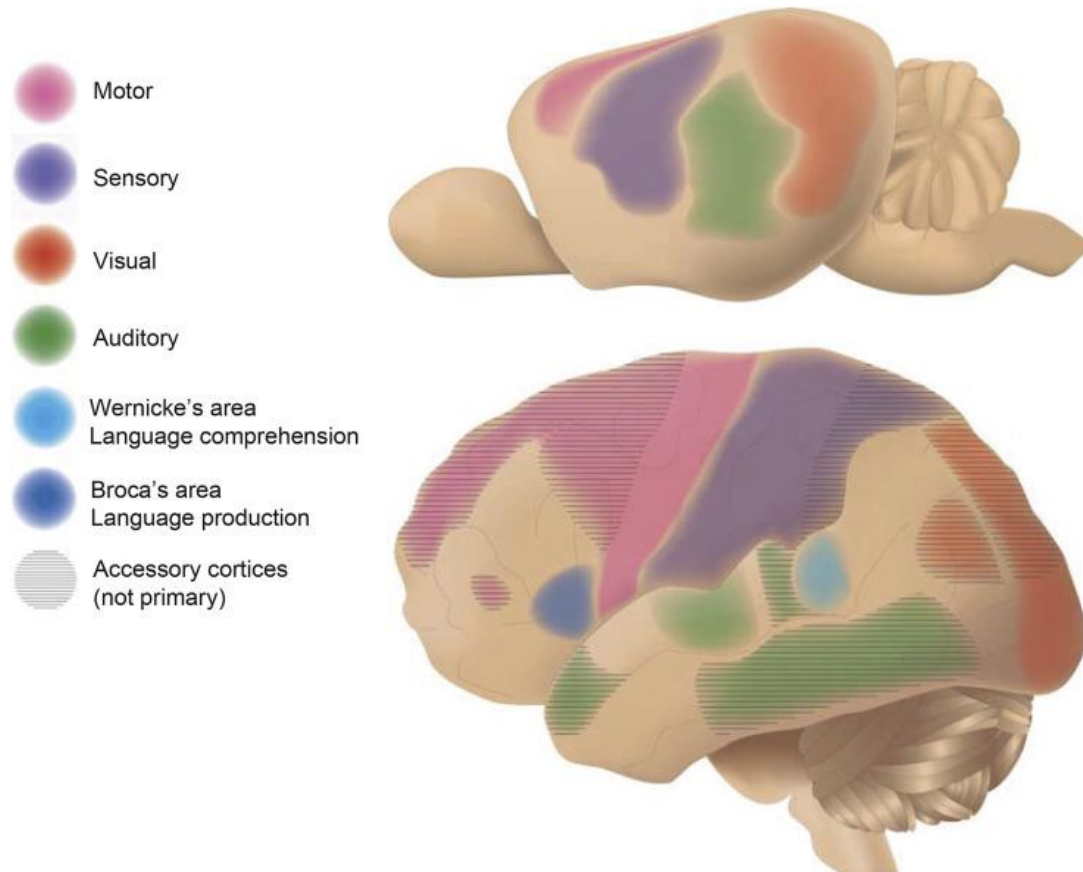
Korbian Brodmann and his pioneering neuroanatomical studies in 1909 understood the importance of comparative brain homology. He used a numbering system to note the homologies between cortical areas of different species, insinuating that the human brain can only be understood by comparison with other mammalian

brains. This underlines the meaning of cytoarchitecture and topography as important arguments in comparative neuroanatomy (Amunts & Zilles, 2010).

Mice are used as the model organism from which to study the functional and structural development of the cerebral cortex. The rodent brain is similar in its overall organization of regional cortical areas to the human brain (Figure 1). Mice are among the most rapidly developing mammals from gestation to young adult and are relatively simple to breed. Advancements in selective breeding, mouse genetics, and the completion of the mouse genome sequence (Waterson et al., 2001) have opened the door for the development of several methods to capitalize on the versatility of the mouse and its malleable genome. Transgenic mouse models are generated when a transgene construct is introduced into the mouse genome. Transgenic mice are commonly used in order to produce a desired protein expression profile both spatially and temporally to study any specific human trait or neurological disorder (Harper, 2010). Postnatal establishment of complex differential gene expression patterns is involved in regionalization of the cortex (O'Leary & Sahara, 2008) which can be functionally analyzed and structurally mapped to investigate the underlying principles of cortical organization. Thus, mice are the model organism of choice for studying mammalian physiology in health and disease.

Figure 1. Comparative brain homology of the human and rodent brains.

The rodent brain has a similar topographical arrangement of functional areas to the human brain. From the rostral to caudal ends of the cortex, the rodent brain (top) shares similar organization to the human brain (bottom) of four primary cortical areas: motor, sensory, auditory, and visual.



Reprinted with permission from Treuting, P. M., Dintzis, S. M., & Montine, K. S. (2018). *Comparative anatomy and histology: A mouse, rat, and human atlas*. London, United Kingdom: Elsevier/Academic Press.

c. Arealization of the Cortex

An important goal of neuroscientists today is to determine the factors controlling the development of functionally and structurally distinct cortical areas in order to develop methods by which to study them. The process subdividing the cortical field into several functional areas is called "arealization". Proper area patterning of the neocortex is a critical developmental event, because cortical areas and their interconnections form the basis for sensory perception, movement control, and behavior (O'Leary & Sahara, 2008). Each area has its own cytoarchitecture, connectivity, and distinct functions (Alfano & Studer, 2012) that are thought to be established by the influence of intrinsic mechanism and extrinsic signaling. The process of cortical arealization starts with the formation of a molecular map from early stages within the ventricular zones, in the form of intrinsic graded expression of transcription factors within neural progenitors (Suárez & Fenlon, 2013) These genetic programs drive the first phase of area specification, but are not solely responsible for the entire organization of the cortex. Thalamocortical axon (TCA) input relays extrinsic signals from the sensory periphery to the cortex to amplify and refine this map. Cortical partitioning and TCA pathfinding may be driven by independent mechanisms, but they are highly correlated and work in conjunction with each other (Alfano & Studer, 2013). The establishment of complex differential gene expression patterns is also involved in postnatal regionalization of the cortex (O'Leary & Sahara, 2008) which can be functionally analyzed and structurally mapped to investigate the underlying principles of cortical organization.

d. In Vivo Functional Recordings Using Calcium Imaging Techniques

To understand how neuronal function develops in the neonatal mouse, it's important to monitor activity during the first 2 weeks of postnatal life. To approach this question, *in vivo* functional recording use the powerful tool of calcium imaging to indirectly measure action potentials through the flux of calcium with a high degree of temporal and spatial resolution. Functional recordings capture the emitted fluorescence of the genetically encoded calcium indicator, GCaMP6s (Lawrence & Heinz, 2011). These mice are designed to have widespread brain expression of GCaMP6s that results in EGFP expression following calcium binding such as in neuronal activation (Zeng et al., 2015). GCaMPs consist of a circularly permuted enhanced green fluorescent protein (EGFP), which is flanked on one side by the calcium binding protein calmodulin and on the other side by the calmodulin-binding peptide M13 (Nakai et al., 2001) In the presence of calcium, calmodulin-M13 interactions elicit conformational changes in the fluorophore environment that lead to an increase in the emitted fluorescence which is captured by a CMOS camera (Grienberger & Konnerth, 2012) (Figure 2).

Functional recordings utilize a mouse line transgenic for Snap25-GCaMP6s (Figure 3). Snap25 is a SNARE protein primarily found in the plasma membrane that can form a complex with other SNARE proteins to promote vesicle fusion in neurons, (Purves et al., 2012) and is expressed by all neurons. In our transgenic mice, GCaMP6s is encoded downstream of the the Snap25 promoter which allows all

neurons to express the fluorescent calcium indicator and thus, total neuronal activity within the entire brain can be monitored.

Figure 2. GCaMP activation in calcium imaging.

GCaMPs are single-fluorophore genetically encoded calcium indicators that consist of EGFP (cpFP) flanked by calmodulin (CaM) and M13. In the presence of calcium, CaM-M13 interactions induce a conformational change that leads to an increase in emitted green fluorescence. The emitted fluorescence can be detected and recorded. (Adapted from Török et al., 2016).

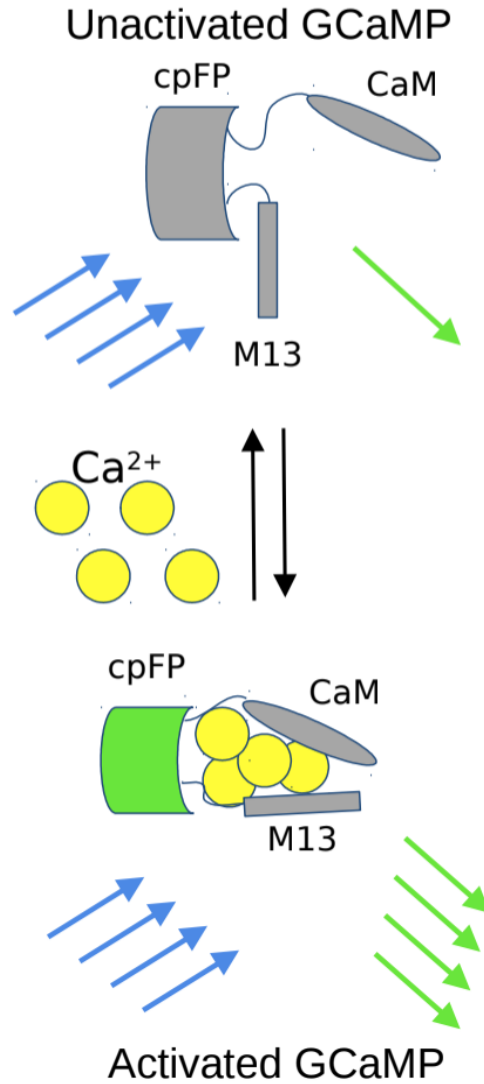
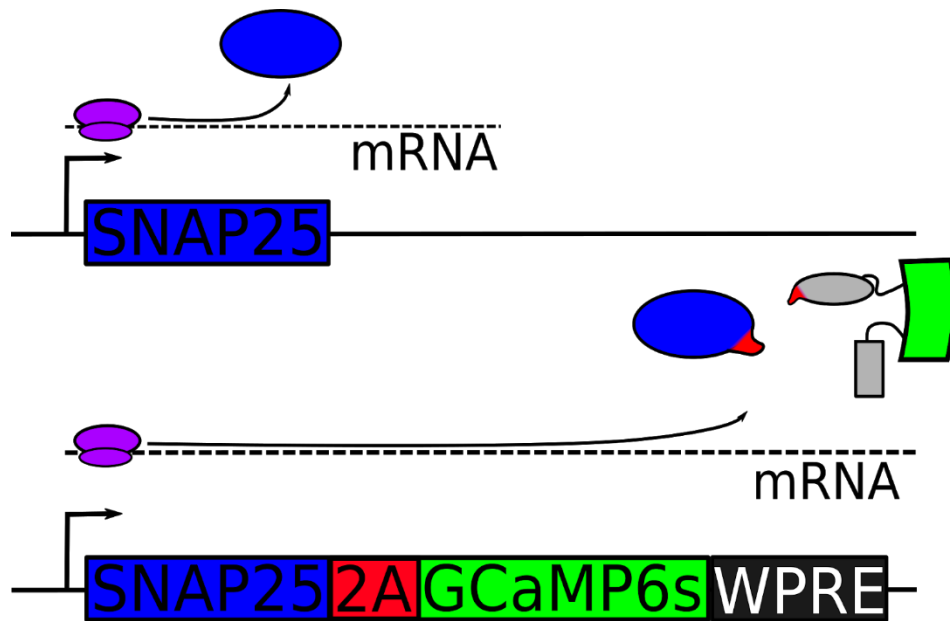


Figure 3. Generation of wild-type and Snap25-GCaMP6s transgenic mouse lines.

(Top) Wildtype mice have normal transcription of the Snap25 gene and are used for structural mapping experiments. (Bottom) Snap25 - GCaMP6s transgenic mouse line used in calcium imaging and functional mapping (Zeng et al., 2015). GCaMP6s is downstream of the Snap25 promoter so all neurons will express the calcium indicator. 2A is a self-proteolytic unit that cleaves Snap25 and GCaMP6 so they will not be fused together. With this, Snap25 is transported as normal to the axon terminals while GCaMP6s fills the entire cell. Woodchuck Hepatitis Virus Posttranscriptional Regulatory Element (WPRE) that creates a tertiary structure when transcribed to stabilize mRNA and prevent degradation.

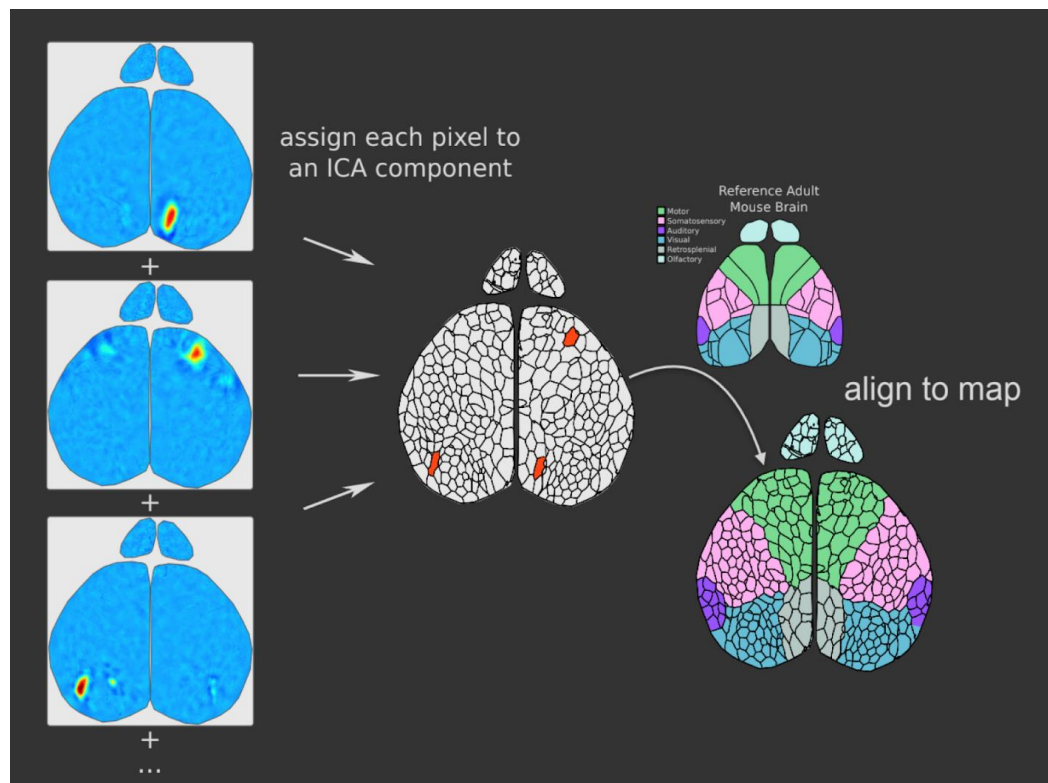


e. Functional Mapping - ICA and Domain Segregation

Independent component analysis (ICA) is a statistical and computational technique for separating a multivariate signal into additive subcomponents (Hyvärinen, 1997). When applied to functional recordings of brain activity, two independent components were revealed - blood dynamics and signal. This technique effectively separated the unwanted blood artifacts from the activity domains captured within the video matrix. These activity domains can be subjected to component domain analysis, which supports the identification of information within components in contexts that are different from which they were originally conceived (Valerio et al., 1997). In the case of our experiments, component domain analysis is performed to make sense of the shape of the activity domains and use that information to map the development of functional structures in the mouse brain, called a functional structure map or domain map. This unbiased functional parcellation of the neonatal mouse cortex has the distinct advantage of flexibility. This approach can be applied to a wide range of ages and genotypes to give a snapshot of the developing functional domains in the cortex (Figure 4).

Figure 4. Creation of functional structure maps by ICA and domain analysis.

A functionally recorded mouse brain can be subjected to independent component analysis, domain parcellation, and alignment to a reference adult mouse brain (Allen Brain Institute) to create maps of functional structure called domain maps. Each activity domain is outlined in black. The collection of these domains within the cortex are aligned to the reference brain to assign them to functional region they are predicted to be associated with (B.R. Mullen, S.C. Weiser, unpublished data).



f. Mapping Regional Cytoarchitecture of Neonatal Mice

One of the central themes of neurodevelopmental studies is to address the issue of how functional changes correlate to regional cortical development. As previously described, data regarding the development of neuronal function can be collected using calcium imaging technology. After those experiments take place, anatomical mapping experiments take place with the aim of providing a structural frame for functional data analyses of the cortex (Amunts & Zilles, 2010). Functional maps generated of the brain during the first 2 weeks of development have consistently demonstrated that functional imaging is predictive of the boundaries of early anatomical structure. To investigate the validity of the maps of functional structure, maps of cytoarchitecture must also be generated as a point of comparison of regional structural boundaries.

Patterns of thalamocortical axon terminals outline primary sensory cortical areas (Lebrand et al. 1996; Ackman et al. 2014) during mouse postnatal development. Referencing functional imaging recordings of *in vivo* brain activity, it is apparent that cortical area patterning begins to stabilize specifically around the end of the first postnatal week. That observation implies that around postnatal day 7 (P7), the cells in those areas are more likely to be forming core groups that behave similarly, which would indicate a possibility of underlying cytoarchitecture of functional areas with distinct cortical localization.

To investigate the variation of cortical dynamics with respect to region and age, whole-mount *in situ* hybridization (WISH) experiments were performed. WISH

is the method of choice to characterize and visualize gene expression patterns in terms of spatial distribution and developmental stage across the whole brain (Chitramuthu & Bennet, 2013). The method of WISH generally occurs in the following steps: (1) the synthesis of a labeled nucleic acid probe complementary to the target mRNA, (2) fixation and permeabilization of tissue, (3) hybridization of the probe to the tissue and washing to remove unhybridized probe, and (4) detection of the probe,” (Nieto, Patel & Wilkinson, 1996). Incorporation of digoxigenin (DIG)-labeled nucleotides into the antisense RNA provides an immunological substrate for probe detection (Antin et al., 2010). cDNA for the target mRNA must be obtained through cloning from cDNA repositories, or from colleagues. After the probe has hybridized to specific mRNA and an antibody binds to the DIG-labeled probe, a color reaction is performed. The DIG-labeled probe is detected by an enzyme-linked immunoassay using an antibody to digoxigenin (anti-DIG) to which alkaline phosphatase has been conjugated (Karcher, 1995). BCIP (5-bromo-4-chloro-3-indolyl- phosphate) is used in conjunction with NBT (nitro blue tetrazolium) for the colorimetric detection of alkaline phosphatase activity. The result of the color reaction is the detectable marking of cortical areas of interest that can be photographed and structurally analyzed.

Different ages in development can show dramatically different expression patterns depending on the target molecule being utilized, the age of the animal, and its genotype. WISH is useful for targeting transcription factors (TFs) that highly regulate the genes responsible for neuronal functionality and cortical organization. (Denkers et

al., 2004) A few examples of these types of TFs are Lmo4, Bhlhb5, and Cux1. Lim- only 4 (Lmo4) is a transcriptional regulator that has been identified in having a central role in establishing the diversity of neuronal subtypes (Macklis et al., 2013) Bhlhb5 is a transcription factor expressed in layers II-IV as a postmitotic regulator of area identity in the developing neocortex. (Joshi et al., 2008) Cux1 is a homeobox transcription factor that is specific to the pyramidal neurons of the upper layers of the murine cortex, suggesting they may define the molecular identity of these neurons (Nieto et al., 2004)

Cadherins are a family of homophilic adhesion receptors that play a role on cell-cell adhesion (Honjo et al., 2000). Recent studies demonstrated that each cadherin shows a spatially restricted expression within specific gray matter structures, and cadherin adhesion functions may provide some kind of code for the selective association of cortical structures during functional differentiation of the nervous system (Redies 2000; Takeichi 2007; Redies et al. 2009). Therefore, targeting Cadherin expression can help us understand the underlying molecular cues regulating cortical regionalization and organization.

Cadherins have been utilized as markers for cortical regions in genetically altered mice at P6, the end of the first week in postnatal development (Grove et al., 2012). The results of those studies were instrumental in my choice of both the target molecule (cadherin 8) and age (P6) to perform my own WISH experiments.

g. Thesis Overview

Distinct functions such as visual perception, motor control, behavior, and planning are allocated to specialized areas (Grove et. al, 2012). The question of how neuronal function changes over the course of development, and how those changes correlate to regional cortical development functionally and structurally is far from fully answered, but advances have been made. *In vivo* recordings of functional brain activity have generated domain maps of the cortex that may provide insight into more complex regional organization that has not been previously reported (Ackman et al., unpublished data). While these domain maps appear to be predictive of underlying anatomical structure, anatomical mapping of regional cytoarchitectural boundaries must be produced to provide a structural frame for functional data analyses.

In this thesis I set out to structurally map the developing mouse cortex at age p6 using the methods of whole mount in situ hybridization. I will also quantify the degree of variation that occurs within a molecular map of the cortex at p6 to provide a basis of comparison for functional maps generated from brains at the same age. Chapter 2 describes the methods and conditions used in all experiments. Chapter 3 explores regional variation of structural maps of p6 brains and the impact of their quantification in understanding how functional areas develop. Chapter 4 will outline future work for this project.

CHAPTER 2

METHODS

a. Snap25-GCaMP6s Transgenic Mice

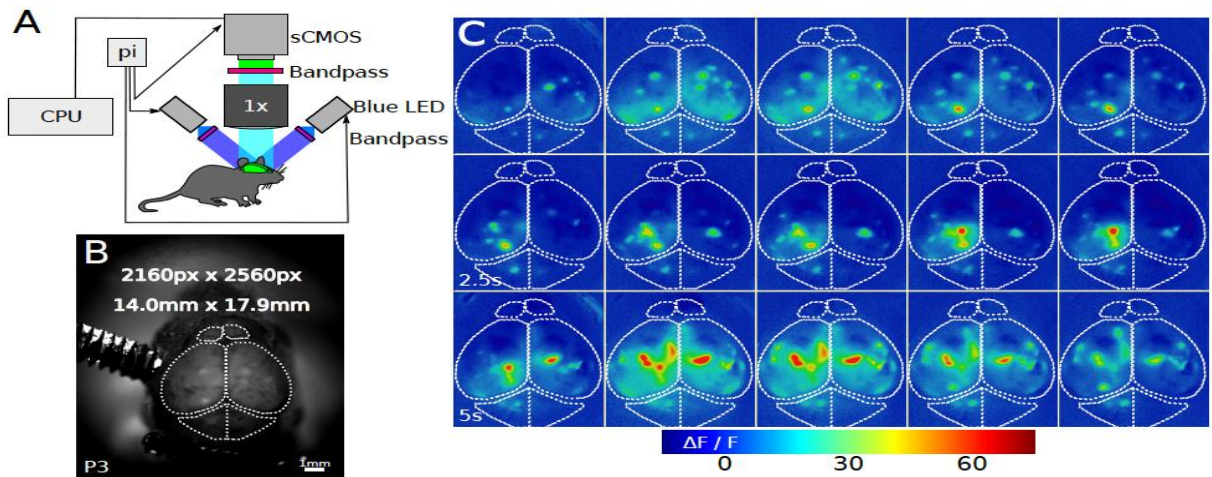
Mice transgenic for Snap25-2A-GCaMP6s-D (025111 - B6.Cg-Snap25) were purchased from The Jackson Laboratory as a calcium-indicator tool strain. This knockin line was generated to express calcium indicator GCaMP6s pan-neuronally to monitor neuronal calcium activity throughout the brain (Zeng et al., 2015). The pan-neuronal expression strategy was adapted from the generation of Cre reporter mice with ubiquitous expression of fluorescent proteins of different spectra (Madisen et al., 2010).

b. Functional Data Acquisition

Calcium imaging technology allows for high quality *in vivo* functional recordings of activity patterns in awake, behaving transgenic mice (Figure 5). The mice are anesthetized, the skin on the skull is removed and the mouse is head mounted onto a steel bar attached to a stage under a camera. When the mouse awakens, the brain is illuminated with blue light to activate GCaMP6s, and its emitted green fluorescence is captured by a complementary metal-oxide semiconductor (CMOS) camera. From the captured image, the change in fluorescence ($\Delta f/f$) is calculated and applied to a color scale, and the subsequent functional imaging recording is produced.

Figure 5. Functional Imaging Set-Up

(A) Schematic of recording system utilizing a CMOS camera coupled to a macro lens to achieve highly sensitive measurements of fluorescent signals together with a large field of view. Transgenic mice express a genetically encoded calcium indicator (GCaMP6s) as a reporter of neuronal activity (Ackman et al. 2014). (B) Single frame of an 10 min video acquired at 10 frames per sec, showing transcranial mouse prep in a postnatal day 3 (P3) animal. (C) Example montage for a segment of the movie in B, showing relative change in baseline fluorescence ($\Delta F/F$). Interval between displayed frames is 0.5s (B.R. Mullen, unpublished data).



c. ICA and Domain Mapping of Functional Brain Data

A video matrix of functionally recorded data is equal to spatial components times component timecourses. ICA was applied to functional recordings resulting in the separation of unwanted blood artifacts from useful spatial components called activity domains. These spatial component's pixel intensities have a characteristic single-tailed gaussian distribution. The independent components are subjected to a threshold, and that output gives a localized domain. When this component domain analysis was applied to the entire brain, all the domains were combined and aligned to the reference adult mouse brain (Allen Brain Institute) to create a domain map of functional structure.

d. Mapping Regional Cytoarchitecture with WISH

i) Brain Preparation

Mice at the age of postnatal day 6 (p6) were transcardially perfused with 1x PBS in DEPC water and 4% PFA. The brains were dissected and left overnight to fix in 4% PFA. The next day, they were rinsed in PBST, dehydrated with a graded methanol (MeOH) series (25%, 50%, 75%, 100%), frozen for at least one hour at -20°C, then rehydrated through the opposite graded MeOH series and rinsed again in PBST. Brains were then digested at 35°C in a concentration of 10µl/ml proteinase K in PBS for 30 minutes, rinsed twice with 20 ml of PBST, and subjected to a 20 minute fixation in at least 10 ml per brain of 4% PFA with 0.2% glutaraldehyde. Brains were rinsed again in PBST to stop the fixation, then transferred to scintillation tubes containing prehybridization solution. They were either stored at -20°C until

ready to use (up to 10 days) or used immediately for prehybridization and hybridization steps (see below).

ii) Probe Design

Protocol for generating digoxigenin (DIG)-labeled probes for RNA in-situ hybridization, as well as the necessary cDNA, was provided by the Feldheim lab. 10 µg of plasmid DNA was linearized with the appropriate restriction enzyme in a 200 µl reaction at 37°C for 2-3 hours. To ensure the digest was complete, approximately 100 ng DNA was run next to 100 ng of uncut plasmid on 2% agarose gel in 50 ml of TAE buffer at 80V for 40 minutes. When the digest was confirmed to be complete, purification of nucleic acids by phenol:chloroform extraction was performed three times. The equal amount of phenol:chloroform was added to the plasmid digest sample and mixed until a white emulsion formed. The mixture was centrifuged at 80% of the maximum speed that the tubes could bear for 1 minute at room temperature. The aqueous phase (containing our DNA) and the organic phase separated, and the aqueous phase was extracted, transferred to a new tube, and subjected to 2 more extractions with phenol:chloroform. When the final aqueous phase was transferred to a new tube, ethanol (EtOH) precipitation was performed. 1/10 of the volume of the solution of 3M sodium acetate was added, and 2 times the volume of 100% ice cold EtOH was added and mixed. The solution was frozen on ice for 15 minutes, centrifuged at 4°C at max speed for 5-10 minutes, then washed in 70% ethanol and re-centrifuged at 4°C at max speed for 5 minutes. The supernatant was discarded and the pellet was dried for 5-10 minutes. Once dry, the pellet was

resuspended in 20 μ l DEPC water and quantitated using the spectrophotometer. This solution was either stored overnight at -20°C or subjected to transcription.

Once ready for transcription, the 2.5 ng of linearized plasmid DNA was added to a transcription reaction (5X transcription buffer, RNASin, 10X DIG rNTP mix, RNA Polymerase, DEPC water) at 37°C for 2-3 hours. RNASin and RNase-free DNase was then added to the solution and it was incubated for 15 minutes at room temperature. The reaction was then added to a Sephadex G50 column, prepared by poking a hole in the bottom of a 0.5 ml eppendorf tube with a hot needle, adding about 0.3 ml of silanized glass wool, adding enough Sephadex beads up to around 0.5 ml and spun for 30 seconds at 3000 rpm until packed to about 0.5 ml and all solution was spun out. Transcription solution was added on top of beads and collected in new 1.5 ml microcentrifuge tube when spun for 3 minutes at 3000 rpm. RNA was then quantitated using the Nanodrop, and EtOH precipitation occurred if necessary to further purify the RNA to get the desired concentration.

iii) WISH

Prepared brains were transferred to prehybridization solution containing the following: 50% deionized formamide, 5X SSC, 2% blocking powder, 0.1% Tween-20, 0.1% CHAPS, 50 $\mu\text{g}/\text{ml}$ yeast RNA, 5 mM EDTA, 50 $\mu\text{g}/\text{ml}$ heparin, and DEPC water. Prehybridizations and hybridizations were carried out in small capped vials in a circular rotator at 22°C below the predicted melting temperature of the probes, or at the indicated temperature, around 65°C . Prehybridization was carried out for at least 2 hours or overnight. DIG-labeled probe was added to fresh prehybridization buffer and

hybridization was carried out overnight. After hybridization, brains were washed three times with 2X SSC with 0.1% CHAPS for 20 minutes, and three times with 0.2X SSC with 0.1% CHAPS for 20 minutes. Both solutions were pre-warmed to the annealing temperature of the probe to reduce background. Brains were then transferred to 12-well plates for increased wash volumes, rinsed twice at room temperature with KTBTw (50 mM Tris-HCL, 150 mM NaCl, 10 mM KCl, 1% Tween-20, MilliQ water) and then incubated on an orbital shaker in 20% sheep serum in KTBTw at 4°C for 2-3 hours. Anti-DIG antibody binding (1:4000) was carried out overnight at 4°C on the orbital shaker. Following antibody incubation, brains were washed five times for 1 hour in KTBTw at room temperature, then incubated in KTBTw at 4°C overnight. Brains were then washed twice for 30 minutes at room temperature in NTMTw (100 mM NaCl, 100 mM Tris at pH 9.5, 50 mM MgCl₂, 0.1% Tween-20, MilliQ water). Color reactions were carried out in NTMTw containing 3 µl of 75 mg/ml NBT in dimethylformamide (DMF) plus 2.3 µl of 50 mg/ml BCIP per 1 ml of NTMTw, scaled up as necessary. Staining reactions were carried out for 20 minutes while covered (in the dark), then 1-4 hours at room temperature uncovered (in the light) on a rotator until signal was visible. Color reactions were stopped and background was decreased by transferring brains to washes in KTBTw, and color reactions could be restarted to react until signal to background was optimized, then rewashed in KTBTw. Staining was permanently stopped with washes in PBS after KTBTw washes. To further decrease background, brains were dehydrated then rehydrated in graded MeOH series followed by a wash and storage in PBS. Brains

were photographed next to a scale bar using the Ackman lab's microscope setup using direct illumination in a petri dish containing PBS. Photographs from WISH experiments were subjected to computational analysis using Fiji.

CHAPTER 3

QUANTIFYING REGIONAL STRUCTURAL VARIATION

a. Introduction

As discussed above, the regionalization of the mammalian cortex is believed to be controlled by a combination of intrinsic factors such as gene expression, environmental factors, and activity dependent circuitry maturation. Recent studies have elucidated methods to target specific molecules known to define and delineate cytoarchitectonic differentiation in the developing cortex. By using whole mount in situ hybridization on P6 mouse brains, the cortex was structurally mapped. These maps are a start to building a developmental profile of the anatomical structure of the cortex during a key window in development in wild-type mice to be used as a reference for maps of different genotypes.

In addition to collecting the data as a structural reference for different genotypes, these maps are able to be used as a reference for the variation of the underlying anatomy of functional maps. To determine the structural variation between brains at P6, these mapped brains were photographed and the determined borders of regions of interest were measured and quantified. By investigating the interplay of function and structure during cortical development, we should be able to increase our understanding the principles of cortical organization.

b. Results

i) Structural Mapping with WISH

Two litters of P6 mice were transcardially perfused, their brains were dissected, and subjected to methods of WISH. The first litter (G2) produced 3 structurally mapped wild-type brains (Figure 6, A-C). The second litter (G3) produced 4 structurally mapped brains, two wild-type (Figure 6, F-G) and two Snap25-GCaMP6s (Figure 6, D-E) that functionally imaged previous to perfusion and dissection. In each case, borders can be determined around the motor cortex (M), primary visual cortex (V1), secondary visual (V2), and certain areas of the barrel cortex. The functionally imaged brains did not display any clear deviation from the expected results seen in wild-type brains as the borders of the regions of interest are still clear and well defined. Each molecular map showed definite borders around ROIs, so all were subjected to computational analysis to determine structural variation.

ii) Quantification of Regional Map Variation

Structural map images were measured and analyzed using Fiji. A reference origin was chosen to set an origin of axis at the point where the two hemispheres begin to split. Then, regions of interest were defined by drawing polygons around the borders of what appeared to be V1, V2, and the motor cortex (M) (Figure 7 A,B - right hem). Those polygons were used as the basis of designing measurement parameters for the quantification variation of molecular maps.

Junction points around the ROIs were chosen to serve as universally identifiable characteristics to define the most extreme edges of each area (Figure 7 A- left hem). The distances and angles from the origin to each characteristic point were

measured and plotted (Figure 8). The polygons around V1, V2, and M were also restricted to bounding boxes (Figure 7 B- left hem). The distance from the origin to the medial, lateral, anterior, and posterior borders of the bounding boxes were measured and graphed (Figure 9).

Figure 6. Structural maps produced by WISH.

WISH was performed on p6 mouse brains targeting Cadherin 8. (A-C) Litter 1, Snap25-GCaMP6s. (D-E) Litter 2, Snap25-GCaMP6s. (F-G) Litter 2, WT.

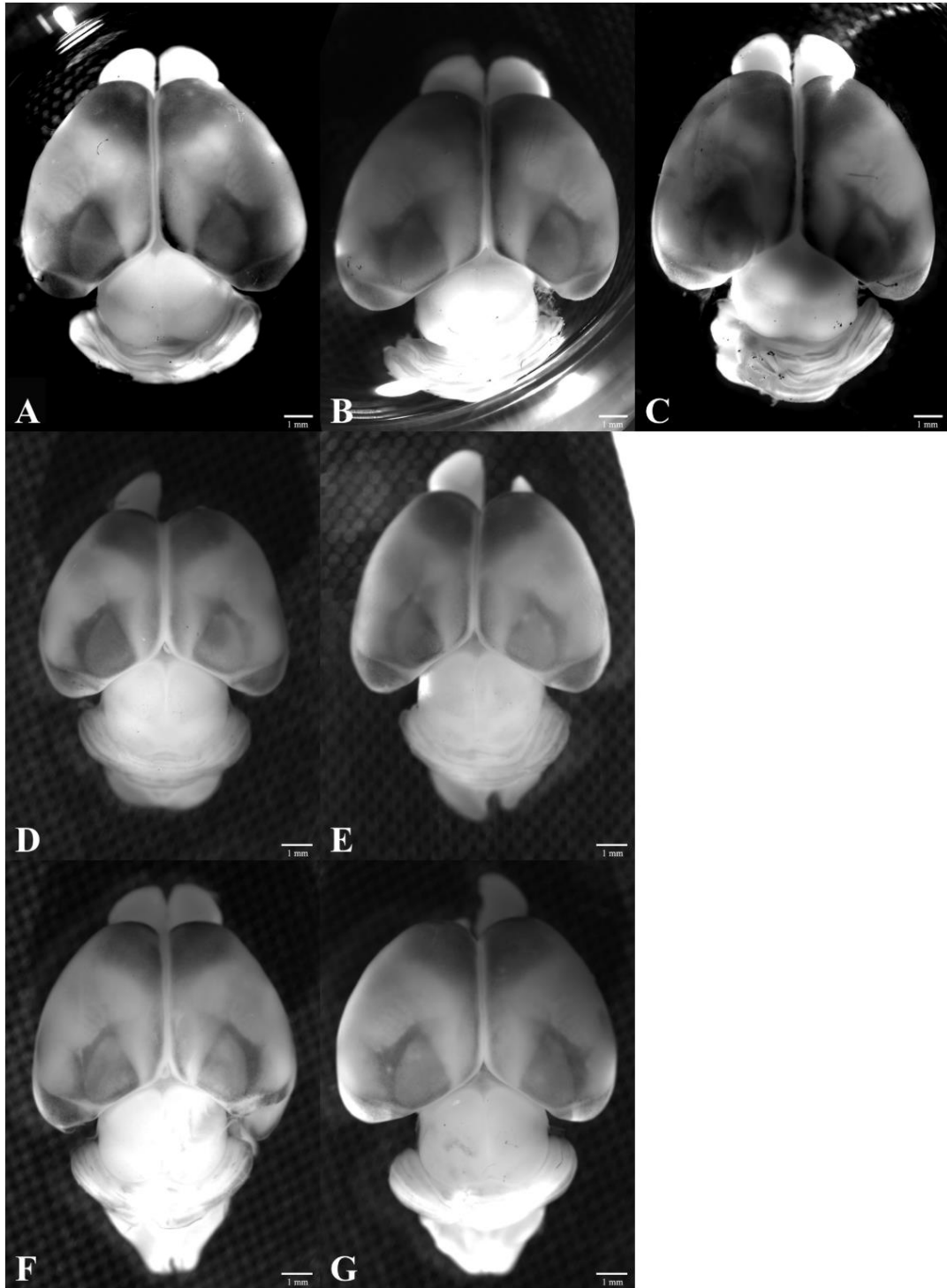


Figure 7. Designing parameters for structural map measurements.

From the raw data images generated by WISH, regions of interest (ROIs) were identifiable as the primary visual (V1, green), secondary visual (V2, blue), and motor cortex (M, orange) on each hemisphere. Polygons were drawn around the borders of each region and their structural variance was quantified by designing two parameters from which to capture their size and location within the cortex: (A) Characteristic points were chosen to delineate the most extreme edges of each ROI. (B) ROIs were restricted to bounding boxes to contain the total borders of each region.

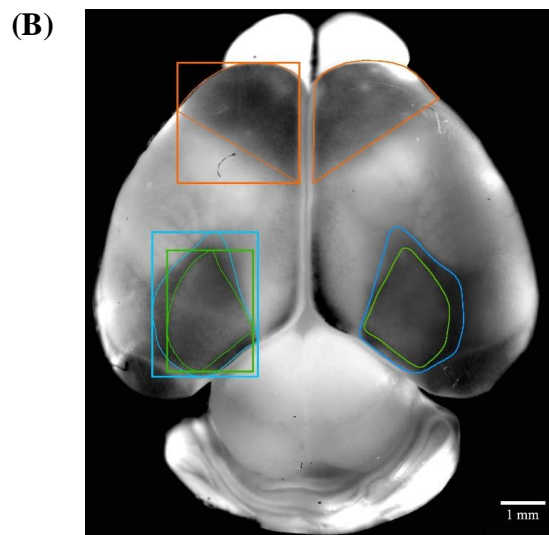
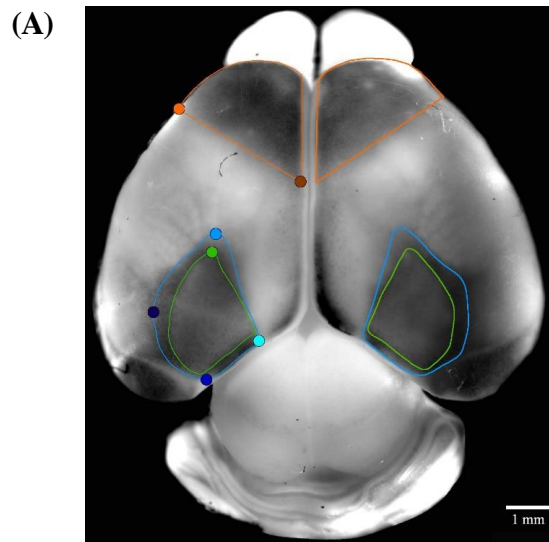


Figure 8. Quantifying length and angle variation from reference midpoint to characteristic edge points of ROIs.

Characteristic points were chosen around ROIs in both hemispheres from each brain. The schematic represents how the distance (red arrow) and angles (yellow curve) from a reference midpoint to each characteristic point were measured. The distance from the midpoint to each characteristic point is plotted against its angle, along with the mean and standard deviation.

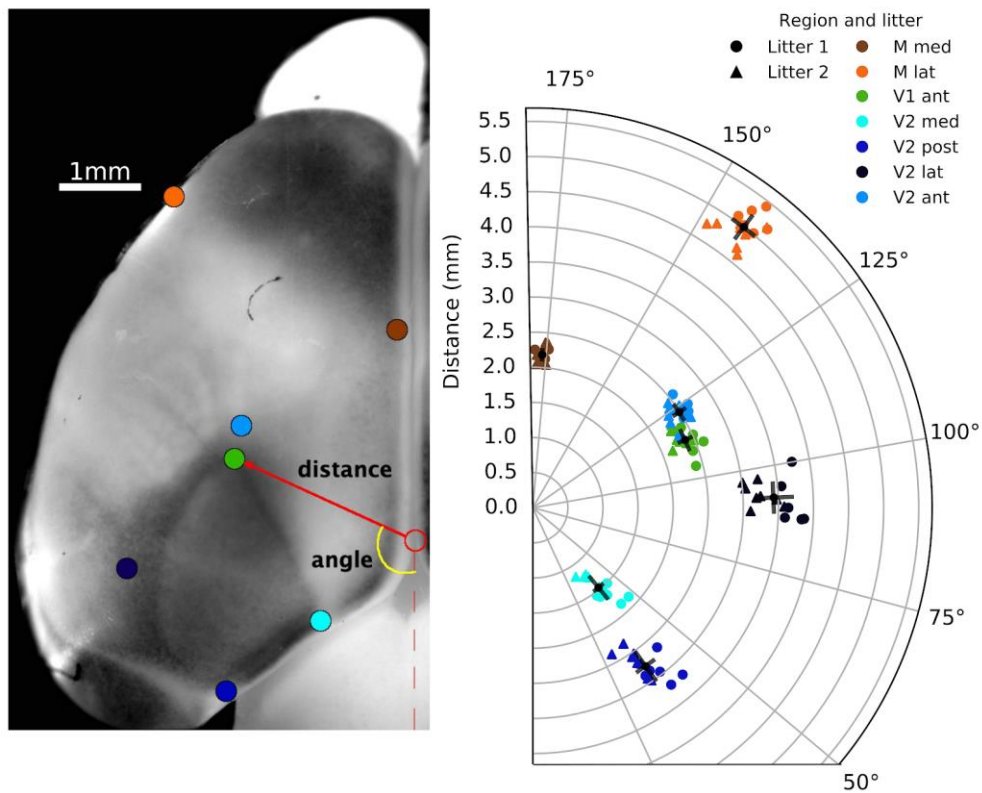
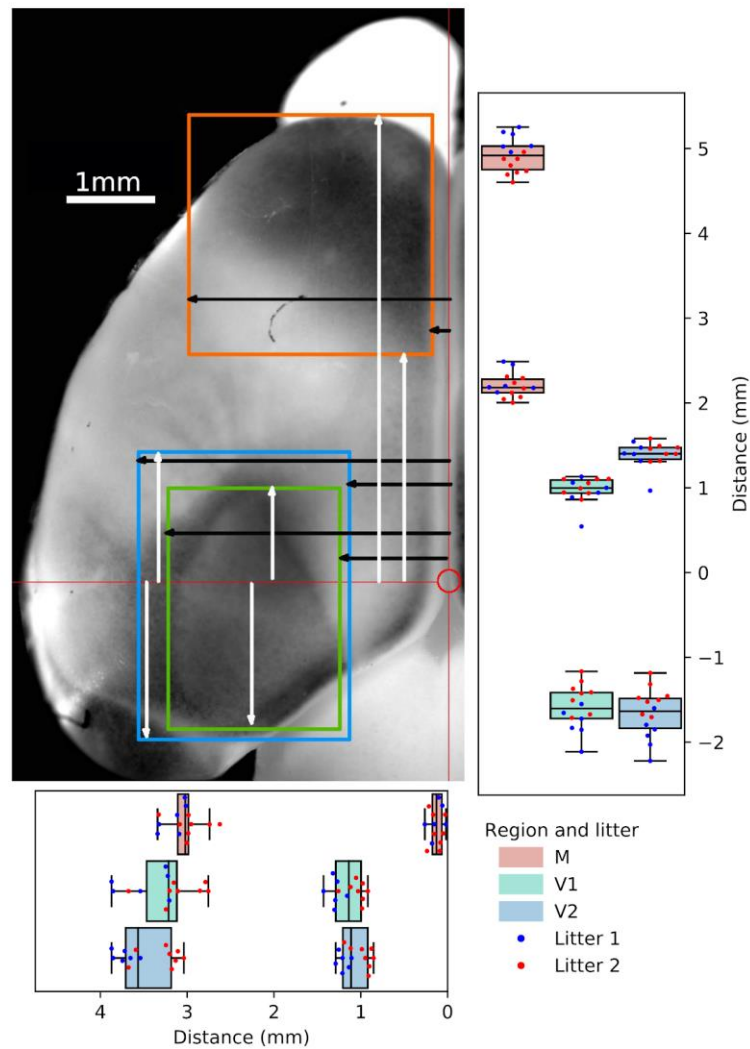


Figure 9. Quantifying medial-lateral and anterior-posterior distance variation of regional bounding boxes with respect to origin axis.

The schematic depicts the method by which the distance from the origin axis (red) to the borders of each bounding box were measured. Black arrows: medial and lateral borders. White arrows: anterior and posterior borders. (Below) Distances from origin to medial and lateral borders. (Right) Distances from origin to anterior and posterior borders.



c. Discussion

i) Potential Sources of Variation

There are many potential sources of variation that can occur during this process of mapping cytoarchitectural boundaries of cortical regions of interest that affect the quality of measurement and distribution of graphed data. From the beginning to end of each procedure, each set of experimental conditions between the two litters can be different in a multitude of ways. The preparation of brain tissue is the start of the workflow, and each individual animal is subject to a unique quality of transcardial perfusion and brain dissection. The perfusion can affect brain swelling and clarity depending on its level of success, and the dissection can cause damage like scratches to the cortical tissue or the accidental removal of an olfactory bulb.

The temperature of the lab when preparing brain tissue and while performing WISH procedures can affect the shrinkage of tissue as well, causing some brains to be larger and therefore measure greater distances between the midline and regions. Every step of WISH requires the incubation of tissue in different solutions. Almost every one of those solutions is made the day of the experiment. For example, prehybridization and hybridization solutions are made to account for the number of brains being incubated, so the volumes of the protocol are scaled down as necessary to both conserve reagents and ensure freshness of the solutions. That being said, the volumes of those solutions used in the incubation of tissue at various steps, while generally kept consistent, can vary slightly. If one brain has slightly less prehyb/hyb solution in its vial while being incubated in the circular rotator, it could get stuck in

the cap which would affect the consistency of tissue areas being submerged and either prepped for probing or actual probe hybridization.

After the probe has hybridized to specific mRNA and an antibody binds to the DIG-labeled probe, a color reaction is performed to convert the colorless compound into a dark purple precipitate (Gilbert & Barresi, 2016). This particular step contains many avenues for variation as its success is defined by the level of dark colorimetric signal relative to background, for which the timing and determination of adequate experimental success is left to the judgement of the individual. After the original color reaction is performed to a degree determined as adequate, signal can further be amplified and background can be reduced by performing a graded series of methanol dehydration and subsequent rehydration incubations for which the timing is also subjective and ill defined. The expected result is a collection of brains marked with dark-colored splotches on the cortical regions of interest and unstained areas of tissue that should not contain the mRNA of the probed target molecule. At this point in the experiment, colorimetrically-marked brains map may appear to be successfully mapped, however real experimental success is determined by the specificity of the demarcated borders around ROIs. To fulfill the overall goal of quantifying regional variability of cortical maps of cytoarchitecture, the borders of ROIs must be consistently identifiable.

The clarity of ROI borders between brains is the basis from which to determine ROI shape and location within the cortex. The ability to identify borders of ROIs is determined first by the success of the color reaction, and finally by the quality

of photograph taken of the brain to be utilized for measurement performance and analysis. It's during photography of the resultant brains that more visible structural variance of the whole brain is revealed. The general shape and size of each individual brain can be affected by so many factors discussed above, such as tissue damage, incubation conditions, and potentially genotype. That being said, the conditions surrounding photography of the tissue can also be a source of variation. Conditions such as the brain's orientation and potential rotation while being imaged, the direction and contrast of lighting on the tissue, as well as the type of container used to house the brain (petri dish, well plate, etc.) during photography influence the raw image produced from which measurement data is collected, and the subsequent graphical distribution of that data.

ii) Analysis of Angles and Distances from Origin to Characteristic Points

Characteristic points were chosen around V1, V2, and M cortical areas to delineate their most extreme edges along anterior, posterior, medial, or lateral boundaries (abbreviated ant, post, med, lat). Figure 8 displays a polar plot of the angle and distance from the origin to each characteristic point from both hemispheres. The points that have the smallest standard deviations (SD) for both measurement parameters are M med (brown), and V1 ant and V2 ant (green and light blue, respectively). These are the locations of the clearest, most consistently identifiable points of each ROI between brains. The lateral corner of M (orange) is the farthest distance from the origin, yet its ratio of SD of angle and distance is relatively equal. This is an interesting discovery as one would expect a higher standard deviation of

distance when it's that far from the starting point. The V2 med (cyan) has a small SD of angle and a larger SD in regards to the distance from that point to the origin. This can be explained by structural differences between brains causing rotation or asymmetry of the hemispheres. Posterior (blue) and lateral (dark blue) points of V2 mark the least distinct outlines of any of the ROIs. This is due mainly to the variance of the color reaction staining between brains, making it difficult to consistently identify those points. The lateral-most edge of V2 was particularly inconsistent in its distinction which explains the wide distribution of graphed points and high standard deviations for both measurement parameters.

The key point of analysis of this graph is that the SD for distance is generally bigger than the SD of the angle of every point. The SD of distance is smaller the closer the point is to the origin, and gets gradually bigger the farther away the point is and the less defined its border is. Variations in the distance from the origin can be explained by differences in brain size or shape, caused by an experimental condition. What's more important is that the in angle from the origin to every point consistently stays below about 3-4 degrees. What this tells us is that the overall variation of the location of ROIs within the cortex is consistently small regardless of differences in brain shape and size.

iii) Analysis of Bounding Box Graphs

ROIs were restricted to bounding boxes in order to analyze each ROI in its entirety. Distances from the origin axis to the medial, lateral, anterior, and posterior

sides of each bounding box are plotted below and to the right of the measurement design schematic to aid with visualization of measurement data collected (Figure 9).

In the anterior-posterior direction, there are two points that are outliers of the distribution of the anterior distances from V1 and V2, and two more points on the bottom edge of the distribution of posterior distances from V1 and V2. I was able to determine the brain and hemisphere responsible for these measurements as the right hemisphere of a WT animal from litter 1 (Figure 6C) by referring to Supplementary Figures 1 and 2. The first factor that may be causing this outlier is that the right hemisphere droops below the left. It's possible that when orienting the photo of this brain for measurement, the midline was rotated clockwise by a few degrees. The staining is very odd in making the midline look like it has a curve, even up close. Another possible explanation for the lobular asymmetry could be that this particular brain got stretched this way during some part of an incubation during the WISH protocol. Either way, when observing this individual brains' bounding boxes with respect to the origin, it becomes obvious how small the distances are to the anterior boundaries and how those outliers came to be plotted as such.

In the medial-lateral direction, there are two brains responsible for data points sitting at the 4th quartile or past it as an outlier for the data set of distances from the origin to the lateral side of M. By once again referring to Supplementary Figures 1 and 2, I deduced that the outlier point is from the measurement of lateral M of the right hemisphere of brain 3 in litter 1, and the point at the edge of the fourth quartile is from the left hemisphere of brain 2 of the same litter. Both brains are transgenic for

Snap25-GCaMP6s. This time, the positioning bounding boxes around M of both brains don't appear abnormal. Instead, these wayward data points can be attributed to a less successful staining of this ROI from the color reaction. It could possibly also be due to issues with the lighting, but regardless, the missing corner of color left me guessing at that outer border more so than compared to brains with dark stained borders of M.

The graphs generated from bounding box measurements display data from both litters in different colors for the sake of visualization. At first glance, there appears to be a separation of the data distribution of the two litters in almost every direction from every ROI (i.e. the two colors aren't well mixed and there seems to be a gap between them). Litter 1 has larger distances from the origin in the medial, lateral, anterior, and posterior directions. While the animals from both litters have been considered to be P6, there is a standard error in birth-time dates of plus or minus half a day since the litters aren't monitored around the clock. This leads me to believe that the larger distances of litter 1 are the result of older brains which would be slightly bigger than litter 2.

To investigate this hypothesis, I considered the brain weights of each animal to see if the brains from litter 1 were significantly bigger and therefore older than litter 2. A T-test was performed to determine if there is significant separation of the data points from litters 1 and 2 using their brain weights (Table 1), which gave a p-value of 0.3, way above the range of significance ($p \leq 0.05$). That result tells me that the

separation is more likely due to variation in measurement experimental conditions as I performed the measurements on the photographs of the two litters on different days.

Table 1. Brain weights of individual animals from each litter.

The brain weights were used to perform a T-test to determine if the apparent segregation in M-L and A-P data distribution between litters 1 and 2 was statistically significant.

Litter	Animal	Genotype	Brain Weight (g)
1	1	Snap25-GCaMP6s	.19
1	2	Snap25-GCaMP6s	.22
1	3	Snap25-GCaMP6s	.22
2	1	Snap25-GCaMP6s	.15
2	2	Snap25-GCaMP6s	.17
2	3	WT	.19
2	4	WT	.23

CHAPTER 4

FUTURE DIRECTIONS

a. LNA Probes: Various Ages and Molecules of Interest

Locked Nucleic Acids (LNAs) are an RNA nucleotide analogue that exhibits superior specificity, hybridization kinetics, and biostability (Darnell & Antin, 2014) compared to antisense RNA probes like the ones utilized in the aforementioned experiments. Moving forward with structural maps, the maximum amount of regional specificity is desired, and we believe that can be achieved using LNAs to probe for other molecules in WISH. The transcription factors *Bhlhb5*, *Lmo4*, and *cux1* as previously described have been shown to produce different patterns across the cortex throughout the first two weeks of postnatal development (Grove et al. 2014; Macklis et al. 2013; Gan et al. 2008; Grove et al. 2012). Targeting multiple different molecules with LNA probes across a wide range of ages will help to build a developmental profile of structure and function to investigate the specific regional formation of functional cortical areas.

b. Genotypic Models of Abnormal Brain Development

These functional and structural mapping methods can be applied to any genotype, and the power of mouse genetics has allowed for the creation of mutant models for a wide variety of developmental disorders.. Any known model of neurodevelopmental disorder can mapped and their structural variation can be analyzed using the wild-type structural maps at the same age as a reference. This will

increase understanding of the underlying mechanisms driving the organization of the nervous system and the structural impacts of abnormal development.

For example, one particular model could target the development of the visual system. Ephrin-A5 (AL-1/RAGS), a ligand for Eph receptor tyrosine kinases, repels retinal axons *in vitro* and has a graded expression in the superior colliculus (SC), the major midbrain target of retinal ganglion cells. *Ephrin-A5*^{-/-} knockout mice were generated that demonstrated retinal axons projecting to topographically incorrect locations (Frisén, et al., 1998). Applying these WISH methods to a model such as that could elucidate the structural variation in regional targets due to the improper guidance of retinal axons in the mammalian brain during development.

c. Aligning Functional and Structural Maps

At P6, mice have not yet opened their eyes (Brust et al., 2015). By saying that our experiments have molecularly mapped V1 at this age, really we're saying that the tissue that is likely going to become V1 has been mapped. We have mapped structure of an area that has not functionally acted as the primary visual cortex because the mouse has not yet opened its eyes. The region we're seeing mapped has been created by spontaneous activity patterns rather than sensory evoked circuitry maturation (Ackman et al., 2014). We are unable to set up any testing of the developing cortex for an animal's response to stimulus because those functional areas (auditory, visual, motor) have not yet "come online".

The most important future goal of these experiments is to align maps of functional structure to maps of their underlying cytoarchitecture (Figure 10). Now

that the structural variance of mice at P6 has been quantified, the variance of domain maps can also be determined by applying the same type of measurements. For example, if we wanted to assess the likelihood of a particular domain's inclusion within the borders of V1, we could look at that domain from the functional map in reference to a molecular map. We could see how much variation exists within a structural map to assign probability that that particular domain falls within the structural boundaries of V1. The diameter of the domain from V1 can be calculated to see if it falls within the calculated area of the anatomically mapped region.

This is exemplified in Table 2 which contains sample data produced from a single animal at p5 where the average domain size from the visual cortex and the motor cortex was calculated using 5 randomly selected domains. Those values can be used to then estimate the number of domains that could theoretically fit within the confines of the calculated areas of the ROIs from structural maps at that same age to see if the shapes and sizes are correlated within similar deviations. Further computational analysis would be applied to quantify and describe aligned patterning.

Figure 10. Comparing functional and structural map variation.

Below is an example of a domain map (left) generated from a functionally recorded P5 animal being compared to a structurally mapped P6 brain (right). The domain map would overlay the map of cytoarchitecture and the resultant coordination would be determined. Scale bar = 1mm. (B.R. Mullen and S.C. Weiser, unpublished data).

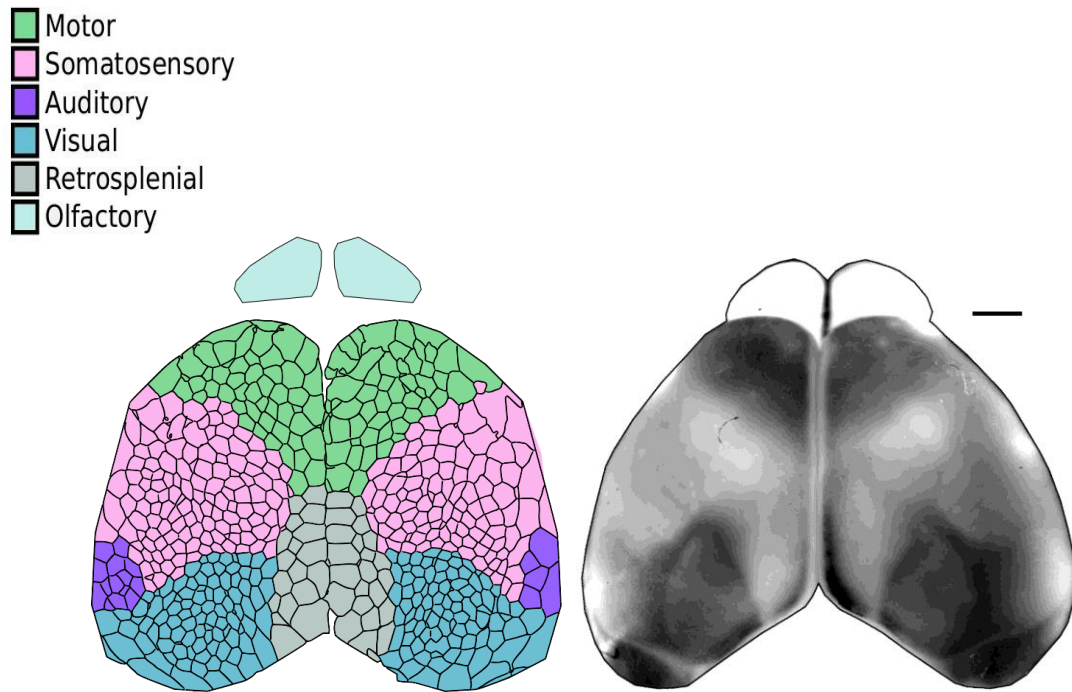


Table 2. Sample data from P5 functional map.

The table displays a sample of the average diameter of and standard deviation of domains from the motor cortex and visual cortex. Values were generated using five randomly selected domains per brain area.

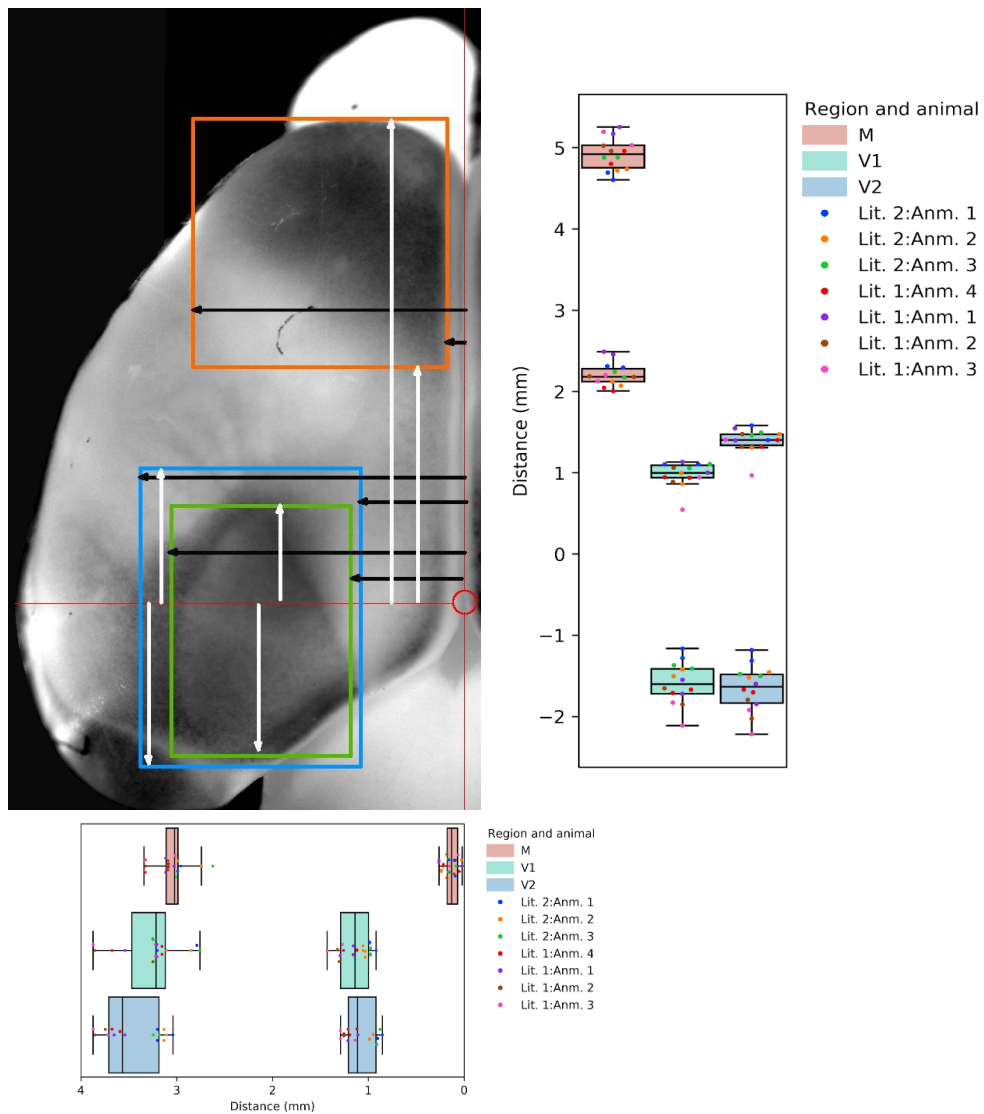
	Average Diameter	Standard Deviation
Motor Cortex	.3062	.0218
Visual Cortex	.2402	.0221

APPENDIX

A. SUPPLEMENTARY DATA AND FIGURES

Supplementary Figure 1. Quantifying medial-lateral and anterior-posterior distance variation of regional bounding boxes with respect to origin axis of individual animals.

These graphs are the same as those shown in Figure 9, except the individual animals are labeled instead of just the litter the points came from. These graphs were necessary to assess the possible sources of variation of the outliers and to analyze the general distribution of the data.



Supplementary Table 1. Compilation of all experimental measurement data utilized

The raw data was referred to in order to determine if the outlier points analyzed from individual animals came from the right or left hemisphere, so then the raw images could be properly assessed for potential sources of variation.

Ang	Dist: ref	Dist: Med Lat	med or lat	Dist: Ant Post	ant or post	ROI	loc	hem	#	GT	litter	Meas M-L	#/lit	Meas A-P
174.7 51	2.3518 26255	3.203 0673 13	Lat	1.101 1567 01	Ant	V1	A	L	1	sn25- gcamp	litter _2	V1 Lat	G2 1	V1 Ant
141.0 2	4.6316 24421	3.203 0673 13	Lat	1.399 0910 71	Ant	V2	B	L	1	sn25- gcamp	litter _2	V2 Lat	G2 1	V2 Ant
119.0 14	2.2525 14798	2.988 0743 79	Lat	4.602 1583 84	Ant	M	C	L	1	sn25- gcamp	litter _2	M Lat	G2 1	M Ant
36.48 3	1.2255 68856	0.918 9038 083	Med	- 1.282 3182 6	Post	V1	D	L	1	sn25- gcamp	litter _2	V1 Med	G2 1	V1 Post
33.69	2.3278 16892	0.852 3323 922	Med	- 1.316 1496 35	Post	V2	E	L	1	sn25- gcamp	litter _2	V2 Med	G2 1	V2 Post
92.52 8	3.1899 71296	0.157 1521 952	Med	2.309 2642 02	Post	M	F	L	1	sn25- gcamp	litter _2	M Med	G2 1	M Post
125.8 82	2.4009 36316						G	L	1	sn25- gcamp	litter _2	nan nan	G2 1	nan nan
175.5 7	2.3572 82929	2.789 4514 65	Lat	1.101 1567 01	Ant	V1	A	R	1	sn25- gcamp	litter _2	V1 Lat	G2 1	V1 Ant
141.8 6	4.7047 43845	3.038 2757 75	Lat	1.580 2526 3	Ant	V2	B	R	1	sn25- gcamp	litter _2	V2 Lat	G2 1	V2 Ant
120.7 16	2.3005 33525	2.954 2430 03	Lat	4.692 7391 63	Ant	M	C	R	1	sn25- gcamp	litter _2	M Lat	G2 1	M Ant
31.87 5	1.1600 88775	0.985 4752 243	Med	- 1.166 6367 83	Post	V1	D	R	1	sn25- gcamp	litter _2	V1 Med	G2 1	V1 Post

28.35 5	2.3703 78945	0.902 5337 879	Med	- 1.184 0981 38	Post	V2	E	R	1	sn25- gcamp	litter _2	V2 Med	G2 1	V2 Post
95.15 2	3.0415 49779	0.090 5807 792	Med	2.292 8941 82	Post	M	F	R	1	sn25- gcamp	litter _2	M Med	G2 1	M Post
127.6 87	2.4369 50361						G	R	1	sn25- gcamp	litter _2	nan nan	G2 1	nan nan
177.0 7	2.1051 84615	3.107 0298 6	Lat	0.993 1145 671	Ant	V1	A	L	2	sn25- gcamp	litter _2	V1 Lat	G2 2	V1 Ant
148.4 71	4.7429 40559	3.107 0298 6	Lat	1.473 3018 3	Ant	V2	B	L	2	sn25- gcamp	litter _2	V2 Lat	G2 2	V2 Ant
114.2 56	2.2939 85517	2.742 5240 74	Lat	4.735 3012 16	Ant	M	C	L	2	sn25- gcamp	litter _2	M Lat	G2 2	M Ant
38.66	1.2681 30909	1.054 2293 1	Med	- 1.424 1917 69	Post	V1	D	L	2	sn25- gcamp	litter _2	V1 Med	G2 2	V1 Post
34.73 1	2.5253 48471	0.987 6578 937	Med	- 1.456 9318 1	Post	V2	E	L	2	sn25- gcamp	litter _2	V2 Med	G2 2	V2 Post
89.08 3	3.1048 47191	0.027 2833 6723	Med	2.119 3719 66	Post	M	F	L	2	sn25- gcamp	litter _2	M Med	G2 2	M Post
124.0 28	2.3365 47569						G	L	2	sn25- gcamp	litter _2	nan nan	G2 2	nan nan
176.3 53	2.0822 66587	2.852 7488 77	Lat	0.861 0630 697	Ant	V1	A	R	2	sn25- gcamp	litter _2	V1 Lat	G2 2	V1 Ant
143.8 12	5.0048 60884	3.133 2218 93	Lat	1.308 5102 92	Ant	V2	B	R	2	sn25- gcamp	litter _2	V2 Lat	G2 2	V2 Ant
112.1 29	2.1532 03342	2.984 8003 75	Lat	4.717 8398 61	Ant	M	C	R	2	sn25- gcamp	litter _2	M Lat	G2 2	M Ant
39.97 1	1.4689 36492	1.031 3112 81	Med	- 1.506 0418 71	Post	V1	D	R	2	sn25- gcamp	litter _2	V1 Med	G2 2	V1 Post

34.76 2	2.6999 62021	0.948 3698 449	Med	- 1.522 4118 91	Post	V2	E	R	2	sn25- gcamp	litter _2	V2 Med	G2 2	V2 Post
92.92 1	3.2489 0337	0.236 8196 275	Med	2.069 1705 71	Post	M	F	R	2	sn25- gcamp	litter _2	M Med	G2 2	M Post
121.6 34	2.3038 07529						G	R	2	sn25- gcamp	litter _2	nan nan	G2 2	nan nan
175.4 17	2.1761 2137	3.244 5380 31	Lat	1.054 2293 1	Ant	V1	A	L	3	WT	litter _2	V1 Lat	G2 3	V1 Ant
143.4 17	4.9579 33493	3.244 5380 31	Lat	1.460 2058 14	Ant	V2	B	L	3	WT	litter _2	V2 Lat	G2 3	V2 Ant
115.2 57	2.2699 76153	3.004 4443 99	Lat	4.878 2660 6	Ant	M	C	L	3	WT	litter _2	M Lat	G2 3	M Ant
38.60 1	1.2604 91566	0.976 7445 468	Med	- 1.370 7163 7	Post	V1	D	L	3	WT	litter _2	V1 Med	G2 3	V1 Post
33.98 6	2.6650 39311	0.910 1731 307	Med	- 1.502 7678 67	Post	V2	E	L	3	WT	litter _2	V2 Med	G2 3	V2 Post
96.79 3	3.0088 09738	0.165 8828 727	Med	2.238 3274 47	Post	M	F	L	3	WT	litter _2	M Med	G2 3	M Post
124.6 58	2.4456 81038						G	L	3	WT	litter _2	nan nan	G2 3	nan nan
178.4 75	2.1772 12705	2.756 7114 25	Lat	1.104 4307 05	Ant	V1	A	R	3	WT	litter _2	V1 Lat	G2 3	V1 Ant
147.0 46	4.8236 99326	3.177 9666 15	Lat	1.492 9458 55	Ant	V2	B	R	3	WT	litter _2	V2 Lat	G2 3	V2 Ant
118.0 25	2.3256 34223	2.623 5685 93	Lat	4.878 2660 6	Ant	M	C	R	3	WT	litter _2	M Lat	G2 3	M Ant
38.35 5	1.2135 64174	0.976 7445 468	Med	- 1.412 1870 88	Post	V1	D	R	3	WT	litter _2	V1 Med	G2 3	V1 Post

33.63 9	2.5548 14507	0.877 4330 901	Med	- 1.478 7585 04	Post	V2	E	R	3	WT	litter _2	V2 Med	G2 3	V2 Post
97.21 6	3.2292 59345	0.082 9414 3637	Med	2.171 7560 31	Post	M	F	R	3	WT	litter _2	M Med	G2 3	M Post
124.9 31	2.5439 0116						G	R	3	WT	litter _2	nan nan	G2 3	nan nan
174.6 59	2.0451 61207	3.675 6152 33	Lat	0.944 0045 061	Ant	V1	A	L	4	WT	litter _2	V1 Lat	G2 4	V1 Ant
140.1 01	5.2002 09794	3.675 6152 33	Lat	1.316 1496 35	Ant	V2	B	L	4	WT	litter _2	V2 Lat	G2 4	V2 Ant
112.7 23	2.4860 60422	3.327 4794 67	Lat	4.800 7812 98	Ant	M	C	L	4	WT	litter _2	M Lat	G2 4	M Ant
41.63 4	1.4951 28524	1.117 5267 22	Med	- 1.713 3954 62	Post	V1	D	L	4	WT	litter _2	V1 Med	G2 4	V1 Post
34.48 4	2.9826 17705	1.117 5267 22	Med	- 1.704 6647 84	Post	V2	E	L	4	WT	litter _2	V2 Med	G2 4	V2 Post
90.26 5	3.5839 43119	0.214 9929 338	Med	2.044 0698 73	Post	M	F	L	4	WT	litter _2	M Med	G2 4	M Post
120.4 28	2.5820 97874						G	L	4	WT	litter _2	nan nan	G2 4	nan nan
178.6 08	2.0451 61207	3.153 9572 52	Lat	0.935 2738 286	Ant	V1	A	R	4	WT	litter _2	V1 Lat	G2 4	V1 Ant
142.0 91	4.9306 50126	3.591 5824 62	Lat	1.399 0910 71	Ant	V2	B	R	4	WT	litter _2	V2 Lat	G2 4	V2 Ant
112.7 27	2.3780 18288	3.086 2945 01	Lat	4.959 0248 27	Ant	M	C	R	4	WT	litter _2	M Lat	G2 4	M Ant
38.9	1.5420 55916	1.258 3088 97	Med	- 1.671 9247 44	Post	V1	D	R	4	WT	litter _2	V1 Med	G2 4	V1 Post

33.95 9	2.9335 07644	1.191 7374 81	Med	- 1.671 9247 44	Post	V2	E	R	4	WT	litter _2	V2 Med	G2 4	V2 Post
91.90 9	3.4780 83654	0.049 1100 6101	Med	2.003 6904 89	Post	M	F	R	4	WT	litter _2	M Med	G2 4	M Post
119.8 36	2.5951 93891						G	R	4	WT	litter _2	nan nan	G2 4	nan nan
174.2 7	2.266	3.54	Lat	0.999	Ant	V1	A	L	2	WT	litter _1	V1 Lat	G3 2	V1 Ant
144.8 09	5.084	3.54	Lat	1.396	Ant	V2	B	L	2	WT	litter _1	V2 Lat	G3 2	V2 Ant
112.8 71	2.47	3.027	Lat	5.17	Ant	M	C	L	2	WT	litter _1	M Lat	G3 2	M Ant
44.55 6	1.51	1.157	Med	- 1.724	Post	V1	D	L	2	WT	litter _1	V1 Med	G3 2	V1 Post
41.72 2	2.662	1.107	Med	- 1.849	Post	V2	E	L	2	WT	litter _1	V2 Med	G3 2	V2 Post
87.75 7	3.595	0.262	Med	2.488	Post	M	F	L	2	WT	litter _1	M Med	G3 2	M Post
121.7 74	2.609						G	L	2	WT	litter _1	nan nan	G3 2	nan nan
179.2 34	2.251	3.206	Lat	1.131	Ant	V1	A	R	2	WT	litter _1	V1 Lat	G3 2	V1 Ant
143.5 81	5.256	3.653	Lat	1.545	Ant	V2	B	R	2	WT	litter _1	V2 Lat	G3 2	V2 Ant
118.4 21	2.4	3.115	Lat	5.253	Ant	M	C	R	2	WT	litter _1	M Lat	G3 2	M Ant
36.07 2	1.546	1.294	Med	- 1.551	Post	V1	D	R	2	WT	litter _1	V1 Med	G3 2	V1 Post
33.87 3	2.881	1.211	Med	-1.6	Post	V2	E	R	2	WT	litter _1	V2 Med	G3 2	V2 Post
94.94 1	3.556	0.019	Med	2.455	Post	M	F	R	2	WT	litter _1	M Med	G3 2	M Post
128.9 77	2.566						G	R	2	WT	litter _1	nan nan	G3 2	nan nan
176.6 68	2.212	3.853	Lat	0.886	Ant	V1	A	L	3	WT	litter _1	V1 Lat	G3 3	V1 Ant
139.8 55	5.185	3.853	Lat	1.316	Ant	V2	B	L	3	WT	litter _1	V2 Lat	G3 3	V2 Ant
109.5 49	2.422	3.324	Lat	5.024	Ant	M	C	L	3	WT	litter _1	M Lat	G3 3	M Ant

42.65 2	1.859	1.321	Med	- 1.854	Post	V1	D	L	3	WT	litter _1	V1 Med	G3 3	V1 Post
38.05 7	3.199	1.254	Med	- 2.028	Post	V2	E	L	3	WT	litter _1	V2 Med	G3 3	V2 Post
87.52 7	3.833	0.179	Med	2.185	Post	M	F	L	3	WT	litter _1	M Med	G3 3	M Post
120.6 39	2.498						G	L	3	WT	litter _1	nan nan	G3 3	nan nan
177.6 3	2.197	3.248	Lat	1.06	Ant	V1	A	R	3	WT	litter _1	V1 Lat	G3 3	V1 Ant
141.1 63	5.016	3.745	Lat	1.473	Ant	V2	B	R	3	WT	litter _1	V2 Lat	G3 3	V2 Ant
114.5 38	2.509	3.091	Lat	4.958	Ant	M	C	R	3	WT	litter _1	M Lat	G3 3	M Ant
37.16 8	1.591	1.303	Med	- 1.655	Post	V1	D	R	3	WT	litter _1	V1 Med	G3 3	V1 Post
35.67 3	2.855	1.212	Med	- 1.796	Post	V2	E	R	3	WT	litter _1	V2 Med	G3 3	V2 Post
90	3.642	0.103	Med	2.177	Post	M	F	R	3	WT	litter _1	M Med	G3 3	M Post
123.8 38	2.657						G	R	3	WT	litter _1	nan nan	G3 3	nan nan
176.6 85	2.147	3.871	Lat	0.941	Ant	V1	A	L	4	WT	litter _1	V1 Lat	G3 4	V1 Ant
142.1 86	5.427	3.871	Lat	1.404	Ant	V2	B	L	4	WT	litter _1	V2 Lat	G3 4	V2 Ant
111.1 94	2.61	3.341	Lat	5.195	Ant	M	C	L	4	WT	litter _1	M Lat	G3 4	M Ant
40.47 5	1.632	1.429	Med	- 1.832	Post	V1	D	L	4	WT	litter _1	V1 Med	G3 4	V1 Post
37.83 3	2.955	1.289	Med	- 1.923	Post	V2	E	L	4	WT	litter _1	V2 Med	G3 4	V2 Post
87.67	3.869	0.154	Med	2.199	Post	M	F	L	4	WT	litter _1	M Med	G3 4	M Post
123.6 9	2.596						G	L	4	WT	litter _1	nan nan	G3 4	nan nan
175.3 1	2.126	3.223	Lat	0.544	Ant	V1	A	R	4	WT	litter _1	V1 Lat	G3 4	V1 Ant
143.2 43	5.021	3.719	Lat	0.966	Ant	V2	B	R	4	WT	litter _1	V2 Lat	G3 4	V2 Ant
104.3 72	2.401	3.016	Lat	5.03	Ant	M	C	R	4	WT	litter _1	M Lat	G3 4	M Ant
47.16 1	1.863	1.27	Med	- 2.113	Post	V1	D	R	4	WT	litter _1	V1 Med	G3 4	V1 Post

41.95 4	3.194	1.137	Med	- 2.221	Post	V2	E	R	4	WT	litter _1	V2 Med	G3 4	V2 Post
100.0 45	3.749	0.061	Med	2.125	Post	M	F	R	4	WT	litter _1	M Med	G3 4	M Post
115.5 6	2.321						G	R	4	WT	litter _1	nan nan	G3 4	nan nan

REFERENCES

- 2002 Release: The Mouse Genome and The Measure of Man. (2002, December).
Retrieved from <https://www.genome.gov/10005831/2002-release-the-mouse-genome-and-the-measure-of-man/>
- Ackman, J. B., Burbridge, T. J., & Crair, M. C. (2012). Retinal waves coordinate patterned activity throughout the developing visual system. *Nature*, *490*(7419), 219-225. doi:10.1038/nature11529
- Ackman, J. B., Zeng, H., & Crair, M. C. (2014). Structured dynamics of neural activity across developing neocortex. doi:10.1101/012237
- Alfano, C., & Studer, M. (2013). Neocortical arealization: Evolution, mechanisms, and open questions. *Developmental Neurobiology*, *73*(6), 411-447.
doi:10.1002/dneu.22067
- Allen Brain Institute. (2011). *Reference Atlas :: Allen Brain Atlas: Mouse Brain*.
Retrieved from <https://mouse.brain-map.org/static/atlas>
- Assimacopoulos, S., Kao, T., Issa, N. P., & Grove, E. A. (2012). Fibroblast Growth Factor 8 Organizes the Neocortical Area Map and Regulates Sensory Map Topography. *Journal of Neuroscience*, *32*(21), 7191-7201.
doi:10.1523/jneurosci.0071-12.2012
- Brust, V., Schindler, P. M., & Lewejohann, L. (2015). Lifetime development of behavioural phenotype in the house mouse (*Mus musculus*). *Frontiers in Zoology*, *12*(Suppl 1). doi:10.1186/1742-9994-12-s1-s17

- Caronia-Brown, G., Yoshida, M., Gulden, F., Assimacopoulos, S., & Grove, E. A. (2014). The cortical hem regulates the size and patterning of neocortex. *Development*, *141*(14), 2855-2865. doi:10.1242/dev.106914
- Cederquist, G. Y., Azim, E., Shnider, S. J., Padmanabhan, H., & Macklis, J. D. (2013). Lmo4 Establishes Rostral Motor Cortex Projection Neuron Subtype Diversity. *Journal of Neuroscience*, *33*(15), 6321-6332. doi:10.1523/jneurosci.5140-12.2013
- Chitramuthu, B. P., & Bennett, H. P. (2013). High Resolution Whole Mount *In Situ* Hybridization within Zebrafish Embryos to Study Gene Expression and Function. *Journal of Visualized Experiments*, (80). doi:10.3791/50644
- Colonnese, M. T., & Shen, J. (2016). Homeostasis of columnar synchronization during cortical map formation. doi:10.1101/075341
- Darnell, D. K., & Antin, P. B. (2014). LNA-Based In Situ Hybridization Detection of mRNAs in Embryos. *Methods in Molecular Biology*, 69-76. doi:10.1007/978-1-4939-1459-3_6
- Denkers, N., García-Villalba, P., Rodesch, C. K., Nielson, K. R., & Mauch, T. J. (2004). FISHing for chick genes: Triple-label whole-mount fluorescence in situ hybridization detects simultaneous and overlapping gene expression in avian embryos. *Developmental Dynamics*, *229*(3), 651-657. doi:10.1002/dvdy.20005

- Fenlon, L. R., & Suarez, R. (2013). Thalamic Afferents and Neocortical Arealization: An Ongoing Journey. *Journal of Neuroscience*, 33(35), 13938-13939.
doi:10.1523/jneurosci.2859-13.2013
- Frisén, J., Yates, P. A., Mclaughlin, T., Friedman, G. C., Oleary, D. D., & Barbacid, M. (1998). Ephrin-A5 (AL-1/RAGS) Is Essential for Proper Retinal Axon Guidance and Topographic Mapping in the Mammalian Visual System. *Neuron*, 20(2), 235-243. doi:10.1016/s0896-6273(00)80452-3
- Gilbert, S. F., & Barresi, M. J. (2016). Chapter 3.10 Techniques of RNA and DNA Analysis. In *Developmental Biology* (11th ed.).
- Grienberger, C., & Konnerth, A. (2012). Imaging Calcium in Neurons. *Neuron*, 73(5), 862-885. doi:10.1016/j.neuron.2012.02.011
- Harper, A. (2010). Mouse models of neurological disorders—A comparison of heritable and acquired traits. *Biochimica et Biophysica Acta (BBA) - Molecular Basis of Disease*, 1802(10), 785-795.
doi:10.1016/j.bbadis.2010.05.009
- Helassa, N., Podor, B., Fine, A., & Török, K. (2016). Design and mechanistic insight into ultrafast calcium indicators for monitoring intracellular calcium dynamics. *Scientific Reports*, 6(1). doi:10.1038/srep38276
- Honjo, M., Tanihara, H., Suzuki, S., Tanaka, T., Honda, Y., & Takeichi, M. (2000). Differential Expression of Cadherin Adhesion Receptors in Neural Retina of the Postnatal Mouse. *Investigative Ophthalmology & Visual Science*, 41(2), 546-551.

- Hyvärinen, A. (1997). *Independent component analysis: A neural network approach*.
Espoo: Finnish Academy of Technology.
- Joshi, P. S., Molyneaux, B. J., Feng, L., Xie, X., Macklis, J. D., & Gan, L. (2008).
Bhlhb5 Regulates the Postmitotic Acquisition of Area Identities in Layers II-
V of the Developing Neocortex. *Neuron*, 60(2), 258-272.
doi:10.1016/j.neuron.2008.08.006
- Karcher, S. J. (1995). *Molecular Biology: A Project Approach*. San Diego: Academic
Press.
- Krishna-K, Nuernberger, M., Weth, F., & Redies, C. (2008). Layer-Specific
Expression of Multiple Cadherins in the Developing Visual Cortex (V1) of the
Ferret. *Cerebral Cortex*, 19(2), 388-401. doi:10.1093/cercor/bhn090
- Lawrence, A. J., & Heinz, A. (2011). Imaging – the interface with pharmacology:
Looking to the future. *British Journal of Pharmacology*, 163, 1563-1564.
doi:10.1111/j.1476-5381.2011.01294.x
- Lebrand, C., Cases, O., Adelbrecht, C., Doye, A., Alvarez, C., El Mestikawy, S., ...
Gaspar, P. (1996). Transient Uptake and Storage of Serotonin in Developing
Thalamic Neurons. *Neuron*, 17(5), 823-835. doi:10.1016/s0896-
6273(00)80215-9
- López-Bendito, G., & Molnár, Z. (2003). Thalamocortical development: How are we
going to get there? *Nature Reviews Neuroscience*, 4(5), 422-422.
doi:10.1038/nrn1131

- Madisen, L., Garner, A., Shimaoka, D., Chuong, A., Klapoetke, N., Li, L., ... Zeng, H. (2015). Transgenic Mice for Intersectional Targeting of Neural Sensors and Effectors with High Specificity and Performance. *Neuron*, 85(5), 942-958. doi:10.1016/j.neuron.2015.02.022
- Mclaughlin, T., Torborg, C. L., Feller, M. B., & O'Leary, D. D. (2003). Retinotopic Map Refinement Requires Spontaneous Retinal Waves during a Brief Critical Period of Development. *Neuron*, 40(6), 1147-1160. doi:10.1016/s0896-6273(03)00790-6
- Nakai, J., Ohkura, M., & Imoto, K. (2001). A high signal-to-noise Ca²⁺ probe composed of a single green fluorescent protein. *Nature Biotechnology*, 19(2), 137-141. doi:10.1038/84397
- Nieto, M. A., Patel, K., & Wilkinson, D. G. (1996). Chapter 11 In Situ Hybridization Analysis of Chick Embryos in Whole Mount and Tissue Sections. In *Methods in Cell Biology* (Vol. 51, pp. 219-235). Elsevier.
- Nieto, M., Monuki, E. S., Tang, H., Imitola, J., Haubst, N., Khoury, S. J., ... Walsh, C. A. (2004). Expression of Cux-1 and Cux-2 in the subventricular zone and upper layers II-IV of the cerebral cortex. *The Journal of Comparative Neurology*, 479(2), 168-180. doi:10.1002/cne.20322
- O'Leary, D. D., & Sahara, S. (2008). Genetic regulation of arealization of the neocortex. *Current Opinion in Neurobiology*, 18(1), 90-100. doi:10.1016/j.conb.2008.05.011

- Pittman, A. J., & Chien, C. (2002). Understanding Dorsoventral Topography. *Neuron*, 35(3), 409-411. doi:10.1016/s0896-6273(02)00797-3
- Purves, D., Augustine, G. J., Fitzpatrick, D., Hall, W. C., LaMantia, A., Mooney, R. D., . . . White, L. E. (2012). *Neuroscience*. New York: Oxford University Press.
- Redies, C. (2000). Cadherins in the central nervous system. *Progress in Neurobiology*, 61(6), 611-648. doi:10.1016/s0301-0082(99)00070-2
- Shen, J., & Colonnese, M. T. (2016). Development of Activity in the Mouse Visual Cortex. *Journal of Neuroscience*, 36(48), 12259-12275. doi:10.1523/jneurosci.1903-16.2016
- Takeichi, M. (2006). The cadherin superfamily in neuronal connections and interactions. *Nature Reviews Neuroscience*, 8(1), 11-20. doi:10.1038/nrn2043
- Treuting, P. M., Dintzis, S. M., & Montine, K. S. (2018). *Comparative anatomy and histology: A mouse, rat, and human atlas*. London, United Kingdom: Elsevier/Academic Press.
- Uchida, N. (1996). The catenin/cadherin adhesion system is localized in synaptic junctions bordering transmitter release zones. *The Journal of Cell Biology*, 135(3), 767-779. doi:10.1083/jcb.135.3.767
- Valerio, A., Succi, G., & Fenaroli, M. (1997). Domain analysis and framework-based software development. *ACM SIGAPP Applied Computing Review*, 5(2), 4-15. doi:10.1145/297075.297081

- Waterson, R. H., Lindblad-Toh, K., Birney, E., Rogers, J., Abril, J. F., Agarwal, P.,
... Brown, S. D. (2001). Initial sequencing and analysis of the human genome.
Nature, 409(6822), 860-921. doi:10.1038/35057062
- Zhuang, J., Ng, L., Williams, D., Valley, M., Li, Y., Garrett, M., & Waters, J. (2017).
An extended retinotopic map of mouse cortex. *ELife*, 6.
doi:10.7554/elifelife.18372
- Zilles, K., & Amunts, K. (2010). Centenary of Brodmann's map — conception and
fate. *Nature Reviews Neuroscience*, 11(2), 139-145. doi:10.1038/nrn2776